solvent mixtures has not been done since it is not available in the literature.

Glossary

S	solubility of CO, m^3/m^3
h	height of the water column in the gas desorption apparatus, m
S_1	solubility of CO at atmospheric pressure and room temperature, m^3/m^3
H	Henry's coefficient of solubility, kmol/(m^3·kPa)
P	barometric pressure, kPa
P_w	vapor pressure of water at T_w, kPa
P_{CO}	partial pressure of CO in the autoclave, kPa
T	temperature in the autoclave, K
T_w	temperature in the gas buret, K
V	volume of water displaced by the desorbed CO gas, m^3
V_1	volume of the liquid sample withdrawn from autoclave, m^3

Registry No. CO, 630-08-0; DMF, 68-12-2; EtOH, 64-17-5; $BuNH_2$, 109-73-9; cyclohexene, 110-83-8.

Literature Cited

(1) Gillies, M. T. *C_1-Based Chemicals from Hydrogen and Carbon Monoxide*; Noyes Data Corporation: Park Ridge, NJ, 1982.
(2) Taqui Khan, M. M.; Halligudi, S. B.; Abdi, S. H. R. *J. Mol. Catal.* **1988**, *45*, 215.
(3) Botteghi, C.; Ganzerla, R.; Lenarda, M.; Moretti, G. *J. Mol. Catal.* **1987**, *40*, 129.
(4) Taqui Khan, M. M.; Halligudi, S. B.; Abdi, S. H. R. *J. Mol. Catal.*, in press.
(5) Chaudhary, V. R.; Parande, M. G.; Brahme, P. H. *Ind. Eng. Chem. Fundam.* **1982**, *21*, 472.
(6) Vogel, A. I. *A Textbook of Practical Organic Chemistry*; Longman: New York, 1978; p 332.
(7) Battino, R.; Clever, H. L. *Chem. Rev.* **1966**, *66*, 395.
(8) Taqui Khan, M. M.; Halligudi, S. B. *J. Chem. Eng. Data* **1988**, *33*, 276.
(9) Dake, S. B.; Chaudhari, R. V. *J. Chem. Eng. Data* **1985**, *30*, 400.

Received for review October 31, 1988. Accepted April 12, 1989.

Solubilities of Carbon Dioxide in Water and 1 wt % NaCl Solution at Pressures up to 10 MPa and Temperatures from 80 to 200 °C

John A. Nighswander, Nicolas Kalogerakis, and Anil K. Mehrotra*

Department of Chemical and Petroleum Engineering, The University of Calgary, Calgary, Alberta, Canada T2N 1N4

Experimental gas solubility data for the CO_2–water and CO_2–1 wt % NaCl solution binary systems are reported. Measurements were made at pressures up to 10 MPa and temperatures from 80 to 200 °C. A thermodynamic model of these systems is also presented. The model employs the Peng–Robinson equation of state to represent the vapor phase and an empirical Henry's law constant correlation for the liquid phase. It is shown that the salting-out effect of the 1 wt % NaCl solution on CO_2 solubility is small. Also described is a new experimental apparatus consisting of a variable-volume equilibrium cell enclosed in a constant temperature controlled oven and the procedure used in conducting the experiments.

Introduction

Carbon dioxide solubility data in water and dilute salt solutions typical of oil-field-produced waters (approximately 1 wt %) are required in the modeling of many enhanced oil and bitumen recovery processes. Applications are also found in geochemical and natural gas systems. In spite of their significance, limited data on the CO_2–water and no data on the CO_2–1 wt % NaCl solution systems are available in the literature.

In the range of temperature and pressure of interest to this study, data for the CO_2–water system were given by Drummond (*1*), Ellis and Golding (*2*), Malinin and Kurovskaya (*3*), and Malinin and Savelyeva (*4*). A summary of the data is provided in Table I. Both Drummond (*1*) and Ellis and Golding (*2*) have reported additional data in the 250–350 °C range. Also, Table I does not include numerous studies that reported solubility measurements at temperatures below 75 °C or at pressure greater than 15 MPa. A summary of these data was provided by Drummond (*1*).

Table I. *PVT* Data for the CO_2–Water System at T = 75–250 °C and P = 1–15 MPa

source	T, °C	P, MPa	no. data pts
Drummond (*1*)	80–250	3–15	34
Ellis and Golding (*2*)	175–250	1.5–9	6
Malinin and Kurovskaya (*3*)	100–150	5	2
Malinin and Savelyeva (*4*)	75	5	1
this work	80–200	2–10	32

The total dissolved solids concentration in a "typical" reservoir produced water is approximately 0.7 wt % (*5*). The solids primarily consist of sodium, potassium, chloride, and bicarbonate ions. On the basis of this, it was decided to perform equilibrium experiments on a synthetic salt solution containing 1 wt % NaCl for which no data exist in the literature. The data available at higher salt concentrations (3–35 wt %) were summarized by Drummond (*1*). At NaCl concentrations greater than 6 wt %, the logarithm of the Henry's law constant, ln (H_g), follows the linear Setschenow relationship with salt concentration. However, it has been shown that the relationship is invalid in the low salt concentration range (*5*).

Thermodynamic models utilizing cubic equations of state are widely used for the modeling of oil and gas phases in petroleum reservoir simulation. However, attempts at modeling the aqueous phase with these equations have concluded that accurate predictions of gas solubility are difficult to obtain (*6–8*). Furthermore, the effect of salts in the water cannot be represented by a cubic equation of state. Instead, empirical Henry's law constant correlations have been used to model the aqueous phase with equations of state used for the oil and vapor phases (*9–13*).

The effect of the inclusion of NaCl on CO_2 solubility has been modeled empirically by Drummond (*1*) and semiempirically by

* Author to whom correspondence should be addressed.

0021-9568/89/1734-0355$01.50/0

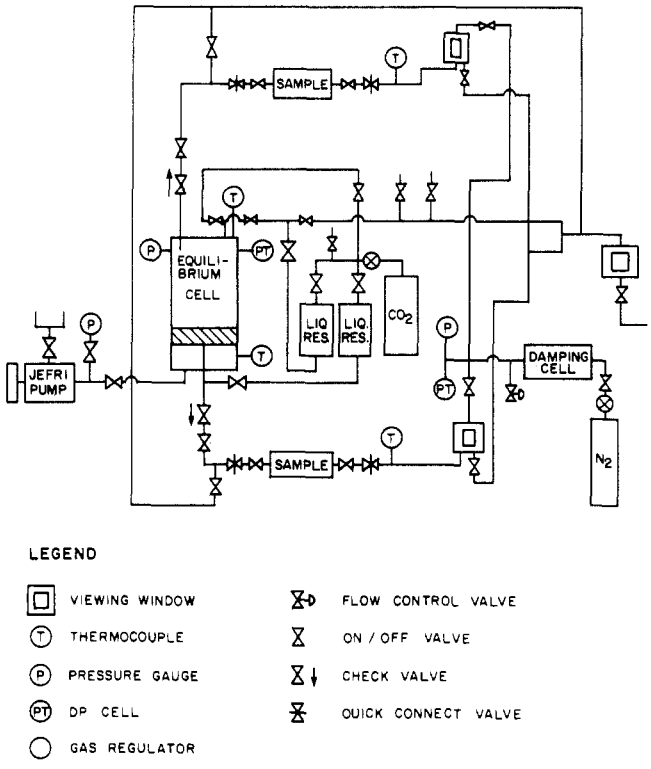

Figure 1. Schematic diagram of experimental apparatus.

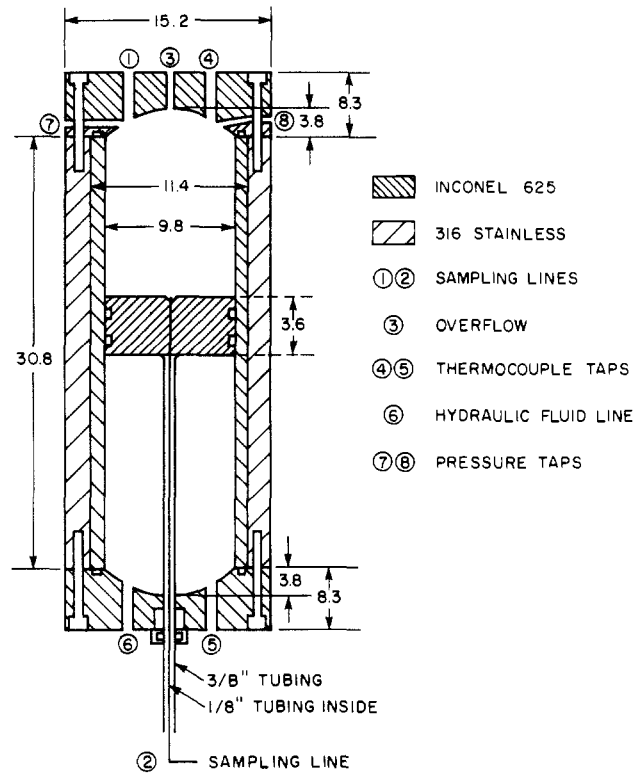

Figure 2. *Equilibrium cell (dimensions in cm).*

Li and Nghiem (*9*) and Barta and Bradley (*14*). These models were based on CO_2 solubility data for more concentrated NaCl solutions (>6 wt %), and they do not accurately predict CO_2 solubility in the 1 wt % NaCl solution (*5*).

In this paper, Henry's law constant correlations for the liquid phase in the CO_2–water and the CO_2–1 wt % NaCl solution systems are used in conjunction with the Peng–Robinson equation of state (PR EOS) (*15*) for the modeling of the vapor phase. It is shown that the proposed model accurately predicts CO_2 solubility in the range of temperature and pressure considered.

Experimental Section

Apparatus. A schematic of the experimental apparatus is shown in Figure 1. The apparatus consists of a 9.8 cm inside diameter equilibrium cell which is constructed of Inconel 625 and fitted with a piston for volume adjustment (Figure 2). The cell is enclosed in a temperature-controlled oven and is attached to a rotating cam device to provide gentle agitation. The cell is fitted with ports for sampling from both the top of the cell and through the cell piston and rod. Cell volume is accurately adjusted by displacing silicone hydraulic fluid to or from the cell with a Jefri high pressure displacement pump.

Two iron–constantan type J thermocouples were used to monitor the cell temperature, one in the upper equilibrium chamber and the other in the lower flange. Calibration of the thermocouples was performed in boiling water, and the agreement obtained was well within the manufacturer's specified accuracy (±0.5%). The deviation in temperature measured at the top and lower flange of the cell was within the specified error for all the tests, indicating that temperature gradients within the cell were negligible.

Cell pressure was monitored with a precision gauge (3-D Instrument Inc.) as well as a Rosemount Alphaline gauge pressure transmitter. Both gauges were calibrated to an accuracy of 35 kPa over the range of operation considered. Both the pressure transmitter and the thermocouple reading were continuously monitored and recorded by use of a SAFE8000 front-end device connected to a supervising microcomputer.

Procedure. Following is a brief description of the experimental procedure used for the vapor–liquid equilibrium (VLE) experiments. Referring to Figure 1, approximately 500 mL of liquid was injected from the liquid reservoir into the equilibrium cell, ensuring complete removal of air bubbles. The cell was then completely sealed and heated to the test temperature. Once thermal equilibrium was achieved, approximately 500 mL of CO_2 at 6 MPa was added from the CO_2 cylinder. The system pressure was then increased to about 11 MPa by inserting the cell piston.

Subsequently, the equilibrium cell was agitated until equilibrium at 10 MPa was achieved. Equilibrium was assumed when no cell pressure variation was observed over a 12-h period. Once equilibrium was reached, agitation was stopped and a sample of the liquid phase was withdrawn for analysis. The piston was then withdrawn to lower the pressure to approximately 8 MPa.

The above procedure was then repeated, decreasing the pressure by 2-MPa steps until the last samples at 2 MPa were collected. The above steps were performed at temperatures of 80, 120, 160, and 200 °C.

Sample Withdrawal. An important consideration in the design of any *PVT* cell is to devise a method to withdraw samples without disrupting equilibrium. This is especially crucial with regard to liquid samples, as the flashing of even a small volume of liquid from the cell can result in a significant reduction in the cell pressure. To avoid this problem we used a novel sampling technique which is described below.

Referring to Figure 1, a back pressure equal to the equilibrium cell pressure was maintained in the sampling line with nitrogen. To obtain a liquid sample, the sampling valve was opened and the piston was very slowly injected, producing a slight increase in the cell pressure. As a result, the sample was forced out against the back pressure and into an approximately 3-mL sampling cell. When sufficient amount of fluid had been withdrawn, as verified by visual observation through the viewing window, the sampling valves were closed and the sample was isolated and removed for analysis. It should be noted that

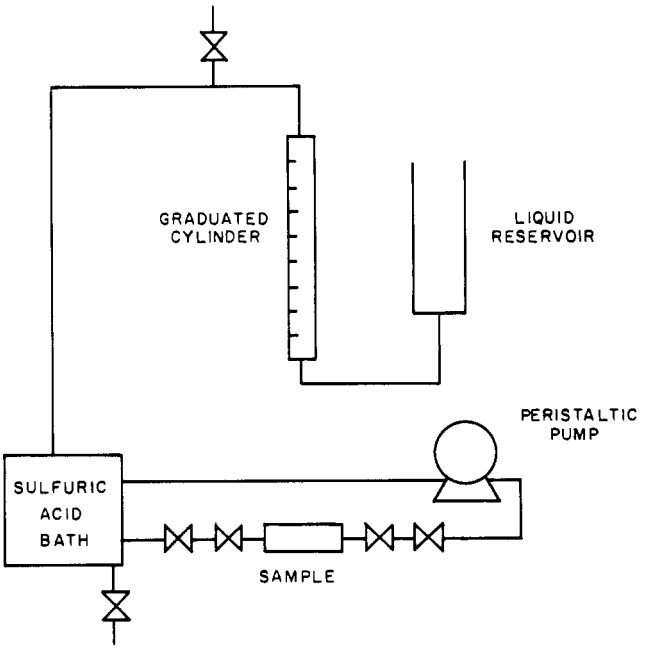

Figure 3. Sample analysis apparatus.

nitrogen was prevented from entering the cell by use of a check valve. Furthermore, the solubility of nitrogen in the liquid is very small (*9*). The back pressure was maintained constant by providing a continuous bleed from the sample line. Pressure fluctuations were kept to a minimum with the help of a large-volume damping cell connected to the sampling line.

Sample Analysis. After a sample cell was removed, it was dried and weighed to an accuracy of 0.001 g. The sample cell was then connected to a depressurization chamber (Figure 3) where the gases evolved from the sample (CO_2 and H_2O) bubbled through a 1 N sulfuric acid solution. Water vapor condensed in the solution, and all the CO_2 escaped the acidic environment and was collected in a volumetric U-tube. The volume of this gas was then determined to an accuracy of 0.5 mL at ambient temperature and barometric pressure. The empty sample cell was then removed from the depressurization cell, dried, and weighed once again. From the mass and carbon dioxide content of the sample, the density and the gas solubility values were calculated.

Error Analysis. In addition to the experimental error involved in sample mass, volume CO_2 evolved, temperature, and pressure measurements, the uncertainty in the sample cell volume must be considered in an overall error analysis for the density and CO_2 solubility measurements. The sample cell volume was calibrated by filling the cell with distilled water and measuring the mass when it was full and empty. From pure water density data (*16*), the sample cell volume was determined as 3.302 cm^3 with a standard deviation of 0.007 cm^3. Using this value as the uncertainty in the cell volume and the results of a typical sample analysis, the standard error in the density and gas solubility measurements were calculated to be 3 kg/m^3 and 0.02 mol %, respectively.

Materials. The carbon dioxide used in all experiments was Coleman Instrument grade with a minimum purity of 99.99%. Water was purified by using a reverse osmosis system to a minimum resistance of 17 MΩ. The synthetic 1 wt % NaCl solution was prepared with Fisher Scientific laboratory grade NaCl with 99.98% purity.

Results and Discussion

CO_2–Water Vapor–Liquid Equilibrium. The first system chosen for study was the CO_2–water VLE. This system was selected due to the availability of previous experimental data,

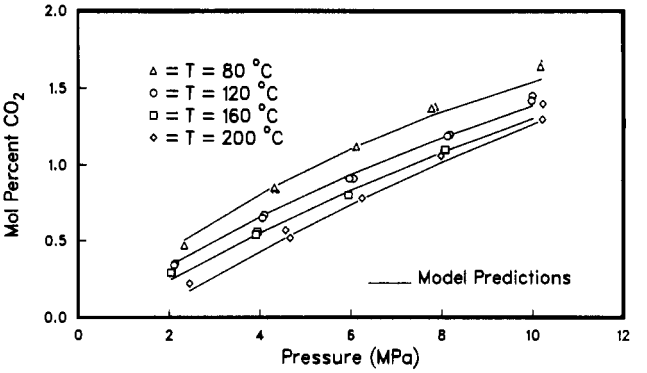

Figure 4. Comparison of CO_2–water solubility data with model predictions.

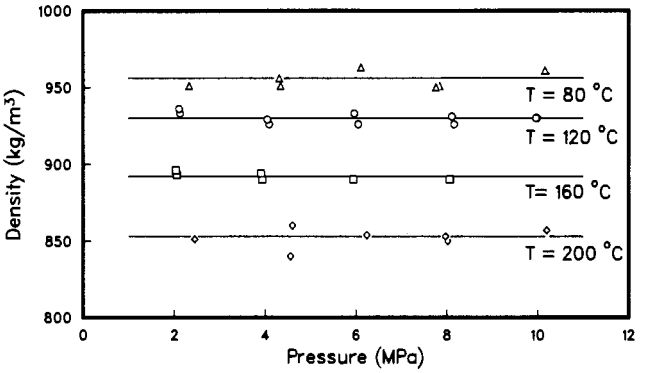

Figure 5. CO_2 saturated water densities.

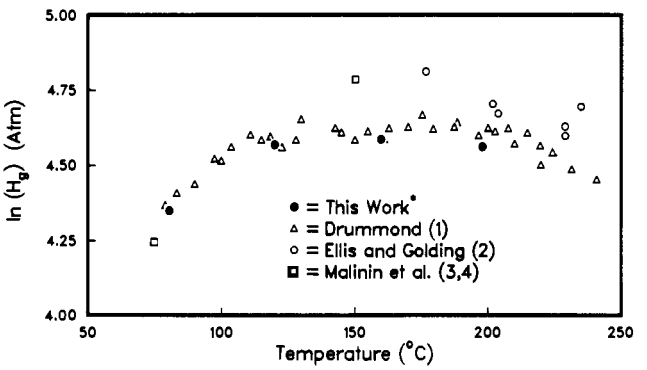

Figure 6. Comparison of carbon dioxide solubility data in water. (*: The data for this work represent the average of 7–10 data points.)

thus making it possible to evaluate both the accuracy and reproducibility of the data from the new experimental apparatus. In this work, experimental density and liquid-phase CO_2 solubility measurements were made at pressures of 10, 8, 6, 4, and 2 MPa for each of the four temperatures of 80, 120, 160, and 200 °C. Results of our experiments are plotted in Figure 4 for the liquid-phase solubility data and Figure 5 for the CO_2 saturated water densities. As shown in Figure 4, the solubility of CO_2 increases with an increase in pressure, but decreases with an increase in temperature. The range of CO_2 solubility is from approximately 0.2 mol % at 200 °C and 2 MPa to approximately 1.7 mol % at 80 °C and 10 MPa. However, the CO_2 saturated water densities do not indicate any pressure dependence. The density values are slightly lower than those for pure water and decrease from 956 kg/m^3 at 80 °C to 853 kg/m^3 at 200 °C. The maximum standard deviation for the density measurements is 6 kg/m^3 or 0.8%.

To compare our data with those reported in the literature, the CO_2 solubilities have been expressed in terms of Henry's law

Table II. Experimental Solubility, Density, and Henry's Law Data for the CO_2–Water System

T, °C	P, kPa	x_g, mol %	m_g, mol/kg	ϕ_i	ρ, kg/m³	ln (H_g), kPa
80.5	2330	0.47	0.262	0.9280	951	8.967
80.2	4310	0.85	0.476	0.8698	956	8.911
80.6	4340	0.84	0.470	0.8695	951	8.930
80.5	6110	1.12	0.629	0.8203	963	8.906
80.5	7760	1.37	0.771	0.7767	950	8.868
80.5	7840	1.38	0.777	0.7746	951	8.868
80.3	10160	1.64	0.925	0.7166	961	8.846
79.7	10180	1.66	0.937	0.7145	961	8.833
		$\overline{\ln (H_g)}$ = 8.891 ± 0.045				
119.9	2110	0.34	0.189	0.9552	936	9.155
120.1	2130	0.35	0.195	0.9549	933	9.135
120.1	4050	0.65	0.363	0.9155	929	9.141
119.9	4090	0.67	0.374	0.9146	926	9.120
120.0	5960	0.91	0.510	0.8785	933	9.144
120.0	6050	0.91	0.510	0.8765	926	9.157
119.9	8110	1.19	0.668	0.8393	931	9.124
120.1	8160	1.20	0.674	0.8387	926	9.111
120.1	9960	1.42	0.799	0.8081	930	9.097
120.3	9980	1.45	0.817	0.8081	930	9.078
		$\overline{\ln (H_g)}$ = 9.126 ± 0.025				
159.7	2040	0.29	0.161	0.9740	896	9.050
159.9	2060	0.29	0.161	0.9738	893	9.061
159.9	3910	0.54	0.301	0.9458	894	9.214
160.0	3940	0.56	0.313	0.9454	890	9.185
159.7	5940	0.80	0.448	0.9177	890	9.249
159.8	8060	1.10	0.617	0.8908	890	9.203
159.8	8070	1.10	0.617	0.8907	890	9.204
		$\overline{\ln (H_g)}$ = 9.167 ± 0.078				
197.8	2450	0.22	0.122	0.9914	851	8.946
198.1	4560	0.57	0.318	0.9648	840	9.107
198.0	4600	0.52	0.290	0.9643	860	9.212
197.7	6240	0.78	0.436	0.9471	854	9.193
198.0	7970	1.06	0.595	0.9313	853	9.166
197.6	8020	1.09	0.612	0.9304	850	9.147
198.1	10200	1.30	0.731	0.9126	857	9.215
198.0	10210	1.40	0.788	0.9124	856	9.141
		$\overline{\ln (H_g)}$ = 9.141 ± 0.087				

constants and these are plotted in Figure 6. The Henry's law constant, H_g, is defined as

$$\ln (H_g) = \ln \left[\frac{\bar{\phi}_g y_g P}{m_g} \right] - \frac{\bar{v}_g^{\infty}(P - P_w^{sat})}{RT} \quad (1)$$

In this equation, the partial molar volume of CO_2 at infinite dilution, $\bar{v}_g^{\infty}$, is estimated as (*1*)

$$\bar{v}_g^{\infty} = 1000\bar{v}_g^{\infty}(\text{at } 25\ ^\circ\text{C})/\rho \quad (2)$$

where $\bar{v}_g^{\infty}$(at 25 °C) is 0.033 m³/kmol (*17*) and ρ is the experimental liquid density. Since at each temperature up to 10 solubility measurements were made, a Henry's law constant was calculated for each point and the average of all these values used as the Henry's law constant for that temperature. The solubility data and the corresponding values of the Henry's law constant for the CO_2–water system are given in Table II. It should be noted that Drummond (*1*) had used the pure component vapor-phase fugacity coefficient and not the fugacity coefficient for CO_2 in the vapor phase mixture as defined in eq 1. To provide a consistent basis for comparison, our data were analyzed using the pure component coefficient and are presented in Figure 6.

As seen in Figure 6, our data agree with the literature values quite well. The data suggest a broad maximum in the Henry's law constant between 150 and 225 °C. It is noted that this maximum in Henry's law constant does not correspond to a minimum in the CO_2 solubility since with increasing temperature the partial pressure ($y_g P$) of CO_2 falls more rapidly than the molality (m_g). Therefore, absolute measurements of solubility should show a minimum in solubility at a temperature higher than that corresponding to the maximum in the Henry's law constant. This explains why the Henry's law constant in Figure 6 decreases beyond 160 °C, while the absolute solubility of CO_2 in water continues to decrease as shown in Figure 4.

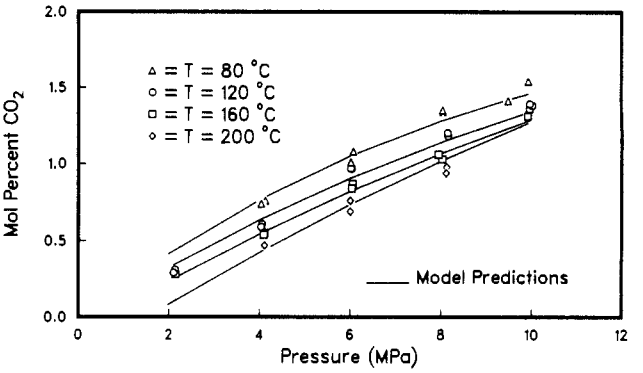

Figure 7. Comparison of CO_2–1 wt % NaCl solution solubility data with model predictions.

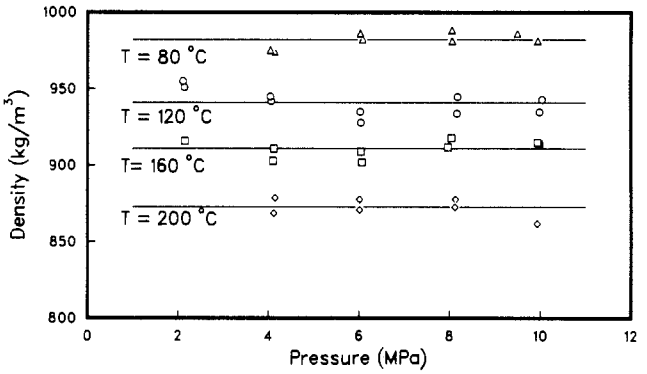

Figure 8. CO_2 saturated 1 wt % NaCl solution densities.

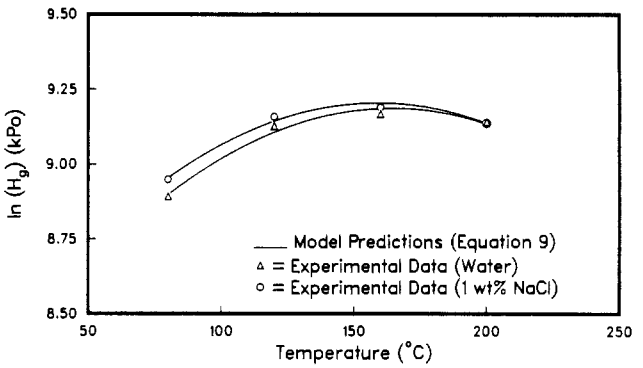

Figure 9. Comparison of data to proposed correlation.

CO_2–1 wt % NaCl Solution Vapor–Liquid Equilibrium. The data obtained for the CO_2 solubility and NaCl solution densities are plotted in Figures 7 and 8, respectively. Comparison of the CO_2 solubility in salt solution with that in water (i.e., Figures 7 and 4) indicates that the solubility is slightly reduced by the inclusion of the salt. It is also observed that the difference in CO_2 solubility between the water and the salt solution becomes smaller with increasing temperature. Also, CO_2 saturated salt solution densities are lower than those for the pure salt solution and show no apparent pressure dependence.

As with the CO_2–water data, the data for the CO_2–1 wt % NaCl solution binary have been reduced in terms of the Henry's law constant as defined in eq 1. In these calculations, the effect of the salt on the vapor pressure of the aqueous phase was approximated as 99.4% of the vapor pressure of pure water at the same temperature. An analysis of vapor pressure

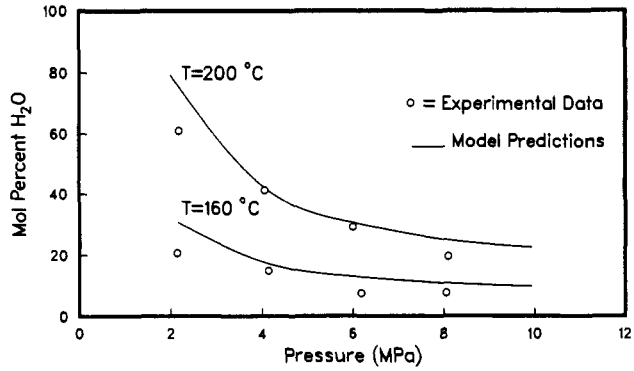

Figure 10. Vapor-phase composition for CO_2–1 wt % NaCl system.

data (*16*) shows this value to be invariant over the range of temperature considered. The solubility data and the values of Henry's law constant for the CO_2–1 wt % NaCl solution system are given in Table III.

The data for both water and 1 wt % NaCl solution are compared in terms of the average Henry's law constant in Figure 9. As seen, the small decrease in solubility due to the presence of the NaCl corresponds to an increase of approximately 0.06 in ln (H_g) at 80 °C and no change at 200 °C.

The vapor-phase compositions for the tests at 160 and 200 °C were also measured, and the results are plotted in Figure 10. The experimental values compare favorably with those predicted by the PR EOS (*15*).

Modeling of CO_2–Water and CO_2–1 wt % NaCl Solution VLE. As mentioned previously, semiempirical models of CO_2 solubility in water and NaCl solutions are available in the literature (*9*, *14*). The model proposed by Li and Nghiem (*9*) involves the use of the PR EOS (*15*) to model the vapor phase. The liquid phase was modeled by modifying Henry's law constant for CO_2 in pure water by the scaled-particle theory to account for the salt (*18–20*). The model of Barta and Bradley (*14*) extended the specific interaction model (*21*) to include gas solubility in brines.

The solubility predictions from both these models begin to show significant error at temperatures beyond approximately 120 °C (*5*). It was also shown by Nighswander et al. (*5*) that these models tend to underpredict the salting-out effect of the 1 wt % NaCl solution. In this paper, an approach similar to that of Li and Nghiem (*9*) has been adopted. Namely, the vapor phase is represented by the PR EOS (*15*) and the solubility in the aqueous phase by Henry's law. The major difference is that the salting-out effect of the 1 wt % NaCl solution has been modeled empirically as opposed to using the scaled-particle theory.

A successive substitution two-phase flash program was used to calculate the vapor–liquid equilibria of the two systems under consideration. The requirement for equilibrium is the equality of fugacity of each component in both liquid and vapor phases

$$f_i^{\mathrm{v}} = f_i^{\mathrm{L}} \tag{3}$$

The vapor-phase fugacities were calculated with the PR EOS (*15*) as

$$f_i^{\mathrm{v}} = \bar{\phi}_i y_i P \tag{4}$$

Interaction coefficients for the CO_2–water system were taken as (*9*)

$$k_{ij} = 0.2 \qquad T \leq 373 \text{ K}$$

$$k_{ij} = 0.49852 - 0.0008(T) \qquad T > 373 \text{ K} \tag{5}$$

For the liquid phase, CO_2 fugacity was calculated by Henry's law

$$f_g^{\mathrm{L}} = H_g^* m_g \tag{6}$$

Table III. Experimental Solubility, Density, and Henry's Law Data for the CO_2–1 wt % NaCl Solution System

T, °C	P, kPa	x_g, mol %	m_g, mol/kg	ϕ_i	ρ, kg/m^3	ln (H_g), kPa
80.3	4040	0.74	0.414	0.8777	975	9.001
80.2	4130	0.76	0.425	0.8750	974	8.983
80.2	6020	1.01	0.566	0.8222	986	8.995
80.2	6070	1.08	0.606	0.8208	982	8.933
80.3	8040	1.35	0.759	0.7691	988	8.904
80.5	8050	1.34	0.754	0.7692	981	8.913
80.0	9490	1.41	0.794	0.7320	986	8.967
80.1	9940	1.54	0.868	0.7214	981	8.899
		$\overline{\ln (H_g)}$ = 8.949 ± 0.042				
120.0	2110	0.29	0.161	0.9553	955	9.304
120.1	2140	0.31	0.173	0.9547	951	9.252
120.1	4040	0.59	0.329	0.9158	945	9.225
120.1	4060	0.61	0.341	0.9154	942	9.197
120.4	6020	0.97	0.544	0.8778	935	9.076
120.1	6040	0.97	0.544	0.8771	928	9.079
120.1	8150	1.20	0.674	0.8389	934	9.106
119.9	8160	1.18	0.663	0.8384	945	9.124
120.0	9970	1.39	0.782	0.8078	935	9.104
120.2	10030	1.38	0.777	0.8072	945	9.116
		$\overline{\ln (H_g)}$ = 9.158 ± 0.080				
160.2	2150	0.28	0.156	0.9724	916	9.128
160.0	4100	0.54	0.301	0.9431	903	9.238
160.1	4120	0.55	0.307	0.9429	911	9.225
159.9	6040	0.84	0.470	0.9165	909	9.185
159.8	6060	0.87	0.487	0.9162	902	9.154
159.9	7950	1.06	0.595	0.8923	912	9.202
160.0	8030	1.03	0.578	0.8914	918	9.241
159.9	9930	1.31	0.737	0.8688	915	9.186
160.1	9970	1.36	0.765	0.8686	914	9.151
		$\overline{\ln (H_g)}$ = 9.190 ± 0.040				
200.0	4120	0.47	0.262	0.9708	869	9.077
200.1	4150	0.47	0.262	0.9705	879	9.086
199.8	6010	0.69	0.386	0.9508	878	9.199
199.9	6010	0.76	0.425	0.9509	871	9.101
199.9	8120	0.94	0.527	0.9317	873	9.237
200.0	8130	0.98	0.549	0.9317	878	9.196
200.5	9930	1.32	0.742	0.9177	862	9.090
		$\overline{\ln (H_g)}$ = 9.141 ± 0.067				

The CO_2 molality is directly related to mole fraction in the liquid phase as

$$m_g = [55.494 x_g/(1 - x_g)] \tag{7}$$

and H_g^* is defined as

$$\ln (H_g^*) = \ln \left[\frac{\bar{\phi}_g y_g P}{m_g} \right] = \ln (H_g) + \bar{v}_g^{\infty} \left[\frac{P - P_w^{\mathrm{sat}}}{RT} \right] \tag{8}$$

where ln (H_g), over the temperature range of 353–473 K and the pressure range from 2 to 10 MPa, is given by the following empirical quadratic expressions:

for pure water

$$\ln (H_g) = 1.384196 + 3.568271 \times 10^{-2}(T) - 4.079688 \times 10^{-5}(T)^2$$

for 1 wt % NaCl solution

$$\ln (H_g) = 1.672958 + 3.487636 \times 10^{-2}(T) - 4.037500 \times 10^{-5}(T)^2 \tag{9}$$

It should be emphasized that H_g has the units of kilopascals and is evaluated by using $\bar{\phi}_g$, the fugacity coefficient of CO_2 in the vapor-phase mixture. Since Henry's law is valid for the solute CO_2, the Lewis–Randall rule applies for the solvent. The fugacity of H_2O in the aqueous phase is determined by the expression

$$f_w^L = x_w \phi_w^{sat} P_w^{sat} \exp\left[\frac{v_w (P - P_w^{sat})}{RT}\right] \quad (10)$$

The molar volume of the water or brine phase, v_w, was calculated from a correlation by Rowe and Chou (*22*). The fugacity coefficient ϕ_w^{sat} was evaluated from the Canjar and Manning correlation (*9*):

$$\phi_w^{sat} = 0.9958 + 9.6833 \times 10^{-5}(T') - 6.175 \times 10^{-7}(T')^2 - 3.08333 \times 10^{-10}(T')^3 \quad \text{for } T' > 90\ ^\circ\text{F}$$

$$\phi_w^{sat} = 1 \quad \text{for } T' \leq 90\ ^\circ\text{F} \quad (11)$$

where T' is the temperature in °F. P_w^{sat} for the salt solution was estimated as mentioned previously to be 99.4% of the value for pure water.

The results of the calculations are shown in Figures 4 and 7 as the calculated lines. Clearly, the model correlates the CO_2 solubility data quite well over the range of temperature and pressure.

Conclusions

A new *PVT* apparatus employing a novel technique for liquid sample withdrawal has been developed and shown to provide accurate and reproducible gas solubility measurements at temperatures up to 200 °C and pressure up to 10 MPa. It was found that CO_2 solubility is slightly lower in a 1 wt % NaCl solution than in pure water due to the salting-out effect.

A model of the CO_2–water and CO_2–1 wt % NaCl solution vapor–liquid equilibria was also presented. The model uses the Peng–Robinson equation of state to represent the vapor phase and a proposed Henry's law correlation for the liquid phase. Predictions are shown to be very good over the range of temperature and pressure considered.

Glossary

f	fugacity, kPa
H_g	pressure-corrected Henry's law constant, kPa
H_g^*	Henry's law constant for CO_2 in water, kPa
k_{ij}	binary interaction parameter in the PR EOS
m_g	CO_2 molality in liquid phase, mol/kg
P	pressure, kPa
R	universal gas constant (8.314 kPa m^3/(kmol K))
T	temperature, K
T'	temperature, °F
v	molar volume, m^3/kmol
$\bar{v}_g^\infty$	partial molar volume of CO_2 at infinite dilution, m^3/kmol
x	liquid-phase mole fraction
y	vapor-phase mole fraction

Greek Letters

ρ	density, kg/m^3
ϕ	pure component vapor-phase fugacity coefficient
$\bar{\phi}$	vapor-phase fugacity coefficient in gas mixture

Subscripts

g	CO_2 component
i	ith component
w	H_2O component

Superscripts

L	liquid
V	vapor
sat	saturated

Registry No. CO_2, 124-38-9; NaCl, 7647-14-5.

Literature Cited

(1) Drummond, S. E., Jr. Ph.D. Dissertation, Pennsylvania State University, 1981.
(2) Ellis, A. J.; Golding, R. M. *Am. J. Sci.* **1963**, *261*, 47.
(3) Malinin, S. D.; Kurovskaya, N. A. *Geochem. Int.* **1975**, *12*, 199.
(4) Malinin, S. D.; Savelyeva, N. I. *Geochem. Int.* **1972**, *5*, 410.
(5) Nighswander, J. A.; Kalogerakis, N.; Mehrotra, A. K. *Proceedings of the 4th UNITAR/UNDP International Conference on Heavy Crude and Tar Sands, August, 1988*; AOSTRA: Edmonton, Canada; p 8:1.
(6) Heidemann, R. A. *AIChE J.* **1974**, *20*, 847.
(7) Peng, D. Y.; Robinson, D. B. *Can. J. Chem. Eng.* **1976**, *54*, 595.
(8) Evelin, K. A.; Moore, R. G.; Heidemann, R. A. *Ind. Eng. Chem. Process Des. Dev.* **1976**, *15*, 423.
(9) Li, Y.; Nghiem, L. X. *Can. J. Chem. Eng.* **1986**, *64*, 486.
(10) Luks, K. D.; Fitzgibbon, P. D.; Bancharo, J. T. *Ind. Eng. Chem. Process Des. Dev.* **1976**, *15*, 326.
(11) Heidemann, R. A.; Prausnitz, J. M. *Ind. Eng. Chem. Process Des. Dev.* **1977**, *16*, 375.
(12) Mehra, R. K.; Heidemann, R. A.; Aziz, K. *SPE J.* **1982**, *22*, 61.
(13) Nghiem, L. X.; Heidemann, R. A. Report CMG R12.02, Computer Modelling Group, Calgary, Canada, 1982.
(14) Barta, L.; Bradley, D. J. *Geochim. Cosmochim. Acta* **1986**, *49*, 195.
(15) Peng, D. Y.; Robinson, D. B. *Ind. Eng. Chem. Fundam.* **1976**, *15*, 59.
(16) Hass, J. L. *U.S. Geol. Survey Bull.* **1976**, *1421-A*, B23.
(17) Reid, R. C.; Prausnitz, J. M.; Poling, B. E. *The Properties of Gases and Liquids*, 4th ed.; McGraw-Hill: New York, 1987; p 336.
(18) Reiss, H.; Frisch, H. L.; Helfand, E.; Lebowitz, J. L. *J. Chem. Phys.* **1960**, *32*, 119.
(19) Lebowitz, J. L.; Helfand, E.; Praestgaard, E. *J. Chem. Phys.* **1965**, *43*, 774.
(20) Pierotti, R. A. *Chem. Rev.* **1976**, *76*, 717.
(21) Pitzer, K. S. *J. Phys. Chem.* **1973**, *77*, 268.
(22) Rowe, A. M.; Chou, J. C. S. *J. Chem. Eng. Data* **1970**, *15*, 61.

Received for review September 26, 1988. Accepted March 17, 1989. We thank the Alberta Oil Sands Technology and Research Authority (AOSTRA) and the Natural Sciences and Engineering Research Council of Canada (NSERC) for the funding of this research.